ISSN 1674-1056
http://cpb.iphy.ac.cn
http://iopscience.iop.org/cpb
中国物理 B
Chinese Physics
中国物理 Chinese Physics B

Pulse generation of erbium-doped fiber laser based on liquid-exfoliated $FePS_3$

Qing Yin(阴晴), Jin Wang(汪进), Xin-Yao Shi(史鑫尧), Tao Wang(王涛), Jie Yang(杨洁), Xin-Xin Zhao(赵新新), Zhen-Jiang Shen(沈振江), Jian Wu(吴坚), Kai Zhang(张凯), Pu Zhou(周朴), Zong-Fu Jiang(姜宗福)

Citation: Chin. Phys. B . 2019, 28(8): 084208. **doi:** 10.1088/1674-1056/28/8/084208
Journal homepage: http://cpb.iphy.ac.cn; http://iopscience.iop.org/cpb

What follows is a list of articles you may be interested in

2-μm-6-μm mid-infrared supercontinuum generation in cascaded ZBLAN and As_2Se_3 step-index fibers

Jinmei Yao(姚金妹), Bin Zhang(张斌), Ke Yin(殷科), Jing Hou(侯静)
Chin. Phys. B . 2019, 28(8): 084209. **doi:** 10.1088/1674-1056/28/8/084209

Zinc-oxide nanoparticle-based saturable absorber deposited by simple evaporation technique for Q-switched fiber laser

Syarifah Aloyah Syed Husin, Farah Diana Muhammad, Che Azurahanim Che Abdullah, Siti Huzaimah Ribut, Mohd Zamani Zulkifli, Mohd Adzir Mahdi
Chin. Phys. B . 2019, 28(8): 084207. **doi:** 10.1088/1674-1056/28/8/084207

Monolithic all-fiber mid-infrared supercontinuum source based on a step-index two-mode As_2S_3 fiber

Jinmei Yao(姚金妹), Bin Zhang(张斌), Jing Hou(侯静)
Chin. Phys. B . 2019, 28(6): 064205. **doi:** 10.1088/1674-1056/28/6/064205

Supercontinuum generation of highly nonlinear fibers pumped by 1.57-μm laser soliton

Song-Tao Fan(樊松涛), Yan-Yan Zhang(张颜艳), Lu-Lu Yan(闫露露), Wen-Ge Guo(郭文阁), Shou-Gang Zhang(张首刚), Hai-Feng Jiang(姜海峰)
Chin. Phys. B . 2019, 28(6): 064204. **doi:** 10.1088/1674-1056/28/6/064204

Generation of wide-bandwidth pulse with graphene saturable absorber based on tapered fiber

Ren-Li Zhang(张仁栗), Jun Wang(王俊), Mei-Song Liao(廖梅松), Xia Li(李夏), Pei-Wen Guan(关珮雯), Yin-Yao Liu(刘银垚), Yan Zhou(周延), Wei-Qing Gao(高伟清)
Chin. Phys. B . 2019, 28(3): 034203. **doi:** 10.1088/1674-1056/28/3/034203

Pulse generation of erbium-doped fiber laser based on liquid-exfoliated $FePS_3$*

Qing Yin(阴晴)[1,3,†], Jin Wang(汪进)[2,†], Xin-Yao Shi(史鑫尧)[3], Tao Wang(王涛)[2], Jie Yang(杨洁)[3], Xin-Xin Zhao(赵新新)[3], Zhen-Jiang Shen(沈振江)[4], Jian Wu(吴坚)[2,‡], Kai Zhang(张凯)[3,§], Pu Zhou(周朴)[2], and Zong-Fu Jiang(姜宗福)[2]

[1] *Nano Science and Technology Institute, University of Science and Technology of China, Suzhou* 215123, *China*
[2] *College of Advanced Interdisciplinary Studies, National University of Defense Technology, Changsha* 410073, *China*
[3] *i-Lab, Suzhou Institute of Nano-Tech and Nano-Bionics, Chinese Academy of Sciences, Suzhou* 215123, *China*
[4] *College of Physics and Electronic Engineering, Hainan Normal University, Haikou* 571158, *China*

(Received 2 April 2019; revised manuscript received 1 May 2019; published online 9 July 2019)

As a preferable material in the field of photo-detection and catalysis, the characteristics of $FePS_3$ in broad wavelength range have been proven by many experimental studies. However, $FePS_3$ has not been used as a saturable absorber (SA) in fiber lasers yet. We propose and demonstrate the generation of a single wavelength and dual-wavelength based on an Er-doped fiber laser (EDFL) at 1.5 μm by using an innovative $FePS_3$ saturable absorber for the first time. The result shows that a stable passively Q-switched pulse can be generated, which demonstrates that the new two-dimensional (2D) material $FePS_3$ served as SA provides a valid method to realize passively Q-switched laser. In addition, we achieve the output of the dual-wavelength pulse by properly rotating the polarization controller. To the best of our knowledge, the dual-wavelength pulse EDFL could be applied in biomedicine, spectroscopy, and sensing research.

Keywords: fiber laser, Q-switched, $FePS_3$

PACS: 42.55.Wd, 42.60.Gd, 78.67.–n **DOI:** 10.1088/1674-1056/28/8/084208

1. Introduction

In the past decade, pulsed fiber lasers have been widely used, such as optical communication, military, material processing, and so on.[1,2] To achieve a simple structure, high beam qualities, and high stability pulsed laser, the saturable absorbers (SAs) have been used. Since the discovery of graphene in 2004, two-dimensional (2D) materials have attracted great attention because of their unique layered structures with weak van-der-Waals forces and excellent mechanical, electrical, and optical properties. In the past few years, various novel 2D materials have achieved rapid development and could be performed as promising SA for ultrafast broadband laser generation on account of their simple fabrication, outstanding saturable laser generation, and outstanding saturable absorption properties, such as ultrafast recovery time and controllable modulation depth.[1,3,4] There are already a series of 2D materials, such as graphene, black phosphorus (BP),[5–8] transition metal chalcogenides (TMDCs, *e.g.*, MoS_2 and WS_2),[9,10] transition metal carbide (*MX*enes, *e.g.*, $Ti_3C_2T_x$),[11–13] and topological insulators (TIs, *e.g.*, Bi_2Se_3).[14]

According to different bandgaps and crystal structures of these 2D materials, it is possible to generate mode-locked or Q-switched pulses at different bands, such as 1 μm, 1.5 μm, 2 μm, 2.8 μm, and 3.4 μm.[15–19] For example, in 2009, Bao *et al.* first used graphene as an SA to achieve mode-locked fiber lasers with broadband and short recovery time.[20] However, graphene is a zero-band-gap material with poor absorption of light (single layer absorption coefficient is only 2.3%), which severely limits its light modulation capability and its application in the field of strong light and matter interactions.[21] Then, TMDC semiconductors represented by MoS_2 have also been widely used as SA in fiber lasers. TMDCs have broadband tunable band gaps and exhibit excellent third-order nonlinear optical properties, but the optical response occurs mainly in the visible to the near-infrared range, which limits its further application.[22,23] In recent years, BP has become a promising candidate for SAs in wide spectral range due to its tunable direct band gap by adjusting the number of layers (from 0.3 eV (bulk) to 1.73 eV (monolayer), corresponding to a wavelength range from 4 μm to 0.7 μm).[24–26] However, black phosphorus is very easily oxidized, which makes it difficult to be widely used in the semiconductor industry and optoelectronic devices.[27,28] Therefore, it makes

*Project supported by the National Natural Science Foundation of China (Grant Nos. 61875223 and 11574349), the Natural Science Foundation of Hunan Province, China (Grant No. 2018JJ3610), the Natural Science Foundation of Jiangsu Province, China (Grant Nos. BK20150365 and BK20170424), and the Natural Science Foundation of Hainan Province, China (Grant No. 117111).

†These authors contributed equally to this work.
‡Corresponding author. E-mail: wujian15203@163.com
§Corresponding author. E-mail: kzhang2015@sinano.ac.cn

© 2019 Chinese Physical Society and IOP Publishing Ltd

sense to develop other new and superior 2D materials used as SA in mode-locked and Q-switched fiber laser.

More interestingly, the ternary layered 2D materials are highly expected to exhibit more novel electrical, optical, and magnetic properties compared with those unary and binary 2D layered materials because of higher chemical diversity and structural complexity.[29] As a family of representative ternary layered 2D materials, metal phosphorus trichalcogenides (MPX_3, M = Fe, Ni, Mn, Co, Zn, Cd, *etc*., and X = S or Se) have received tremendous attention and could be applied in various fields.[30,31] There are several obvious characteristics for MPX_3. (i) These materials show a layered monoclinic crystal structure and each unit cell includes two cations and one $[P_2X_6]^{4-}$ cluster, forming a hexagonal lattice. (ii) Anisotropic properties and magnetic or antiferromagnetic properties.[32] (iii) Due to the changes of the metal and chalcogenide atoms, the band gaps of MPX_3 bulks can range from 1.3 eV to 3.5 eV ($FePS_3$: 1.5 eV,[33] $MnPS_3$: 3.0 eV,[34,35] $NiPS_3$: 1.6 eV,[36] $ZnPS_3$: 3.4 eV,[37] $CdPS_3$: 3.5 eV,[37] $FePSe_3$: 1.3 eV,[38] $MnPSe_3$: 2.5 eV[39,40]), which suggests their optical and electrical applications of photo-detection and photo-catalysis in a broad wavelength range. However, MPX_3 has not been used as SA in fiber lasers yet.

In this work, we report and demonstrate a Q-switched Er-doped fiber laser at 1.5 μm based on an innovative $FePS_3$ saturable absorber. High-quality single crystals of $FePS_3$ are first prepared by chemical vapor transport (CVT) method and then prepared into SA by electrochemical stripping. The experiment demonstrates that the new 2D material $FePS_3$ served as SA provides a valid method to realize passively Q-switched laser. When the pump power is in the range of 20 mW–120 mW, the stable pulse train can be observed on the oscilloscope. By properly rotating the polarization controller, we could achieve the output of dual-wavelength pulse, which can be applied extensively in industrial processing and medical devices.[41,42]

2. Sample preparation and characterization of $FePS_3$ saturable absorber

2.1. Crystal growth and characterize of $FePS_3$

The high-quality $FePS_3$ crystals were fabricated by a CVT method, using iodine as a transport agent. The stoichiometric amount of iron powder (Fe, 99.99%), red phosphorus (RP, 99.999%), and sulfur (S, 99.99%) corresponding to 2 g of $FePS_3$ and iodine (I_2, 1 mg/mL) were put in a quartz ampule (20 mm×150 mm; thickness: 2 mm) and sealed under high vacuum (under 1×10^{-3} Pa) using oxygen/hydrogen welding torch, as shown in Fig. 1(a). Then, the ampule was placed in a tube furnace with dual temperature zones and heated at 700 °C for two weeks. Both the heating rate and the cooling rate were 2 °C/min. After it cooled down to room temperature, black hexagonal crystal flakes with metallic luster could be obtained. It can be distinctly seen from the scanning electron microscopy (SEM) image in Fig. 1(c) that $FePS_3$ has a layered structure and the layers are connected together according to the van der Waals interaction so that the $FePS_3$ nanosheet can be obtained by mechanical peeling or liquid phase stripping. To determine the elemental composition of the prepared $FePS_3$ crystals, a piece of $FePS_3$ is randomly selected (Fig. 1(b) (i)–(iv)), and the energy dispersive spectrometer (EDS) element mappings show that the composition of $FePS_3$ is homogenous and the stoichiometric ratio of $FePS_3$ is similar to 1:1:3.

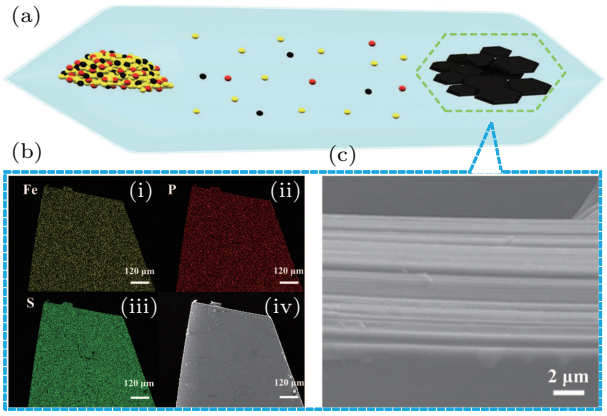


Fig. 1. (a) Schematic diagram of the preparation process of $FePS_3$ crystals. (b) EDS element mappings for: (i) Fe, (ii) P, and (iii) S, as well as (iv) SEM image of a randomly selected $FePS_3$ crystal. (c) The side view SEM image of single-crystalline $FePS_3$.

To further determine the crystal quality of $FePS_3$, the microstructure information and composition information of $FePS_3$ were detected by transmission electron microscopy (TEM) and EDS. The TEM image in Fig. 2(a) shows that the $FePS_3$ nanosheet has a regular shape, consistent with the SEM results. The high-resolution TEM (HRTEM) image in Fig. 2(b) exhibits clear lattice points and the interplanar spacing is 2.84 Å, corresponding to $(13\bar{1})$ planes of $FePS_3$. Figure 2(c) is the corresponding selected area electron diffraction (SAED) pattern recorded along the [101] zone axis; the regular diffraction spots imply that $FePS_3$ flakes are single crystals with excellent quality. Moreover, the high-angle annular dark field (HADDF) image (Fig. 2(c)) and EDS element mappings for Fe, P, and S (Figs. 2(e)–2(g)) indicate that $FePS_3$ flakes have homogeneously composition in the whole scanning area (marked by the yellow region in Fig. 2(d)).

A Raman spectrum is also used to characterize the $FePS_3$ flakes, as shown in Fig. 3(a). Obviously, there are five characteristic vibration modes located at 154 cm^{-1}, 222 cm^{-1}, 244 cm^{-1}, 276 cm^{-1}, and 377 cm^{-1}. The E_g vibration mode at 154 cm^{-1} is attributed to the vibration of the Fe atoms inside the crystal, while the vibration modes of the remaining four positions including the two E_g vibrations and the two A_{1g} vibrations are caused by the vibration of the $[P_2S_6]^{4-}$

cluster, which is consistent with those reported in previous experiments.[43] Figure 3(b) is an x-ray diffraction (XRD) pattern of $FePS_3$ flakes, which is in full agreement with the standard powder diffraction file (PDF) card 30–0663.[44] The most dominant diffraction planes in Fig. 3(b) are at 13.8°, 27.7°, 42.4°, and 57.6°, which correspond to the (001), (002), (003), and (004) crystal planes of $FePS_3$, respectively. This indicates that $FePS_3$ flakes have good crystallinity. To estimate the optical properties of the $FePS_3$ flakes grown by a two-step CVT method, the ultraviolet-visible absorption spectrum was used. The results (shown in Fig. 3(c)) show that the $FePS_3$ flakes have a large amount of absorption of ultraviolet light, and these flakes also have a certain absorption at the wavelength near 1550 nm.

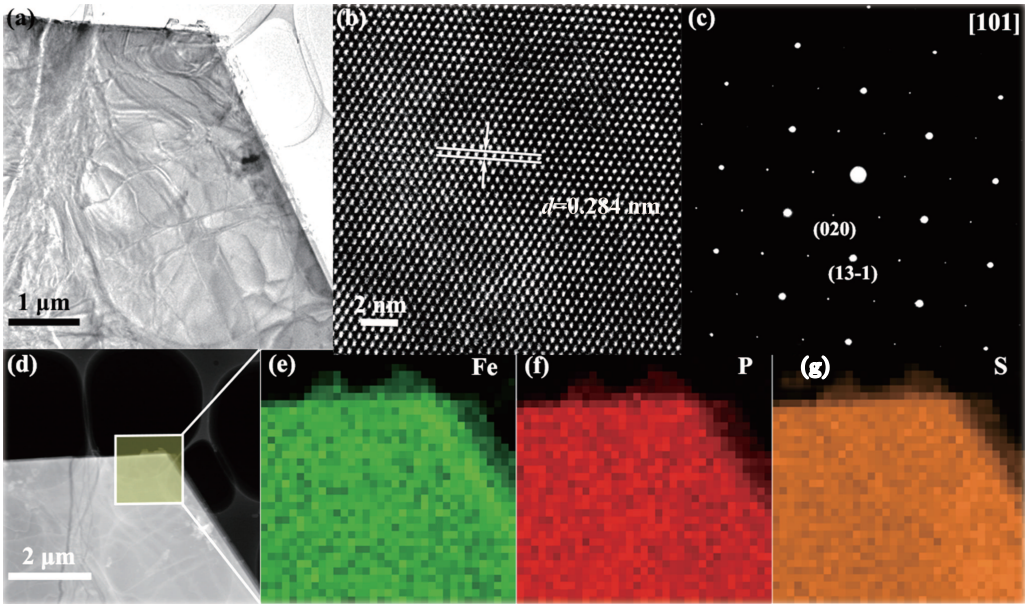


Fig. 2. (a) The TEM image of a piece of $FePS_3$ nanosheet by random search. (b) The HRTEM image for this $FePS_3$ nanosheet. (c) The corresponding SAED pattern. (d) The corresponding HAADF image of the $FePS_3$ nanosheet. (e)–(g) EDS element mappings for Fe, P, and S.

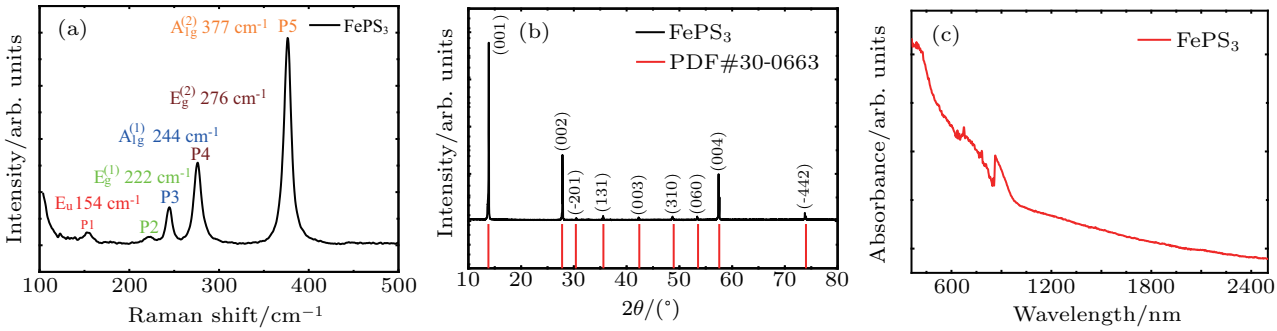


Fig. 3. (a) Raman spectrum and (b) XRD of $FePS_3$ flakes grown by a two-step CVT method. (c) The ultraviolet-visible absorption spectrum of $FePS_3$ nanosheets.

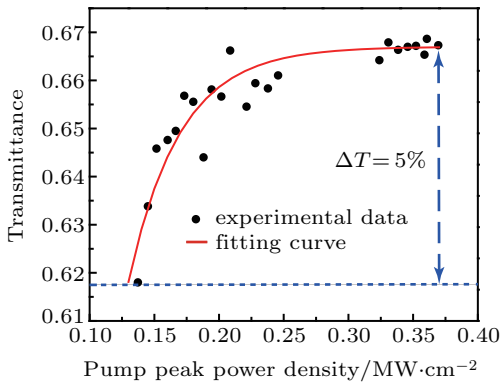


Fig. 4. Nonlinear transmission of the $FePS_3$ film under different incident power intensities.

The saturable absorption properties of $FePS_3$ thin film were also characterized. As illustrated in Fig. 4, the transmittance of the SA under different incident light power intensity was recorded. The laser source we used is a home-made mode-locked Er-doped fiber laser, which has the wavelength of 1559.5 nm, the repetition rate of 150.2 MHz, and a pulse duration of 1 ps. The fitted modulation depth and saturated intensities are 5% and 0.16 MW/cm^2, respectively.

2.2. Preparation of $FePS_3$ SA

The crystals were soaked in ethanol for 2 h to remove the transport agent I_2. After that, clean crystals were put in about 30-mL N-methyl-2-pyrrolidone (NMP) and then sonicated for at least 2 hours. Then, the solution of few-layers

$FePS_3$ nanoflakes could be obtained. Finally, NMP solvent was removed by centrifugation and $FePS_3$ nanoflakes were redistributed in ethanol. The obtained $FePS_3$ nanoflakes solution was then dripped onto the end face of a fiber adapter to form the SA device.

Figure 5(a) is an atomic force microscopy (AFM) image of $FePS_3$ nanoflakes. The $FePS_3$ nanoflakes not only have a size of about 5 μm and a uniform thickness, but also the surface of the samples is clean and free of holes or impurities. The thickness of the sample, as shown in Fig. 5(b), is approximately 31 nm.

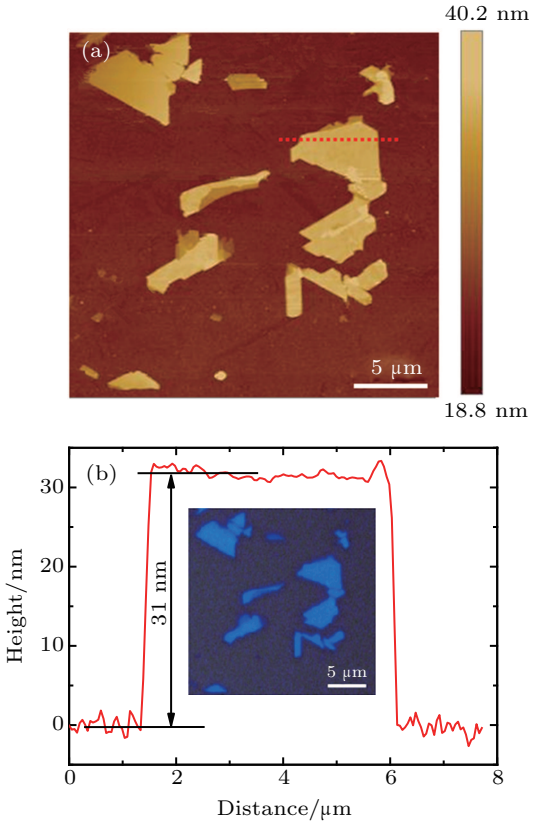


Fig. 5. (a) AFM image of $FePS_3$ nanoflakes; (b) the corresponding height and optical microscope image.

3. Generation of an ultrashort fiber laser

3.1. Experiment setup

A schematic of the configuration of the passively Q-switched ring fiber laser is shown in Fig. 6. The total length of the ring cavity is 15 m, including a piece of 2-m-long erbium-doped fiber (EDF) which plays the role as the gain medium. The fiber laser is pumped by a 980-nm laser diode (LD) with the maximum output power of 900 mW. As a connector, a 980/1550-nm wavelength division multiplexer (WDM) links the seed laser and the EDF together. At the same time, the WDM is connected to the laser cavity, ensuring that the light can propagate in the fiber laser. After the EDF, the polarization-insensitive isolator (ISO) is connected. On the one hand, the ISO ensures the generated signal laser spread through single direction; while on the other hand, it can reduce the filtering effect which exists in the ring cavity with the cavity birefringence. In order to change the polarization state of the circulating, we can adjust the polarization controller (PC) by properly rotating it. At the end of the PC, a 10/90-output coupler is connected to the saturable absorber, the structure of which looks like a sandwich device by smearing the $FePS_3$ on the adapter of the fiber connector. 10% of the energy enters a 20/80-output coupler which is used to test the signal laser by the optical spectrum analyzer and an oscilloscope. Meanwhile, the remaining 90% of the energy passes through the SA.

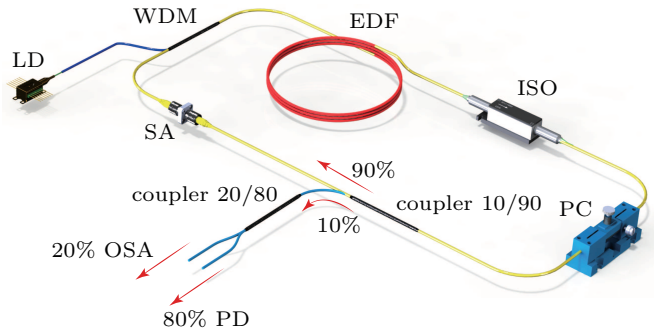


Fig. 6. Schematic diagram of the Er-doped all-fiber ring cavity pulsed laser based on $FePS_3$ thin-film SA.

3.2. Single wavelength output

In the experiment, when the pump power is increased to 20 mW, the pulse trains can be observed on the oscilloscope. By increasing the pump power, stable passively Q-switched performance is realized when the pump power is in the range of 20 mW–120 mW. However, the passively Q-switched operation would become unstable if we continue to increase the pump power. In our previous publication, we identified some of the reasons for this phenomenon, including the over-saturation of the $FePS_3$ SA at high pump power. Another possible reason is that the SA has been damaged under the high pump power. The experiment has been repeated six times to examine whether the $FePS_3$ SA is destroyed. Through repeated experiments, when the pump power is between 20 mW and 120 mW, the stable passively Q-switched performance can always be obtained, which means that the over-saturation of the SA at high incident intensity leads to the instability.

Figure 7 illustrates the performance of the output pulse at a pump power of 100 mW. As shown in Fig. 7(a), the central wavelength is 1559.9 nm with the 3-dB bandwidth of 0.04 nm. Figures 7(b) and 7(c) show the pulse trains and single pulse profile, respectively. The period of pulse trains is 16.67 μs with the single pulse duration of 2.74 μs, giving a repetition rate of 60 kHz (Fig. 7(d)). Figure 7(d) shows the stability of the passively Q-switched pulse with a signal-to-noise ratio of ∼ 62.98 dB. And the inset of Fig. 7(d) shows the radio frequency (RF) spectrum over a large range of 600 kHz. Figure 8(a) shows the relationship between the output power and

the pump power. It is found that there is a positive correlation between them. Figure 8(b) illustrates the changes in the repetition rate and pulse duration as the pump power increases. This shows that the repetition rate rises as the pump power rises. In contrast, the pulse duration decreases as the pump power increases.

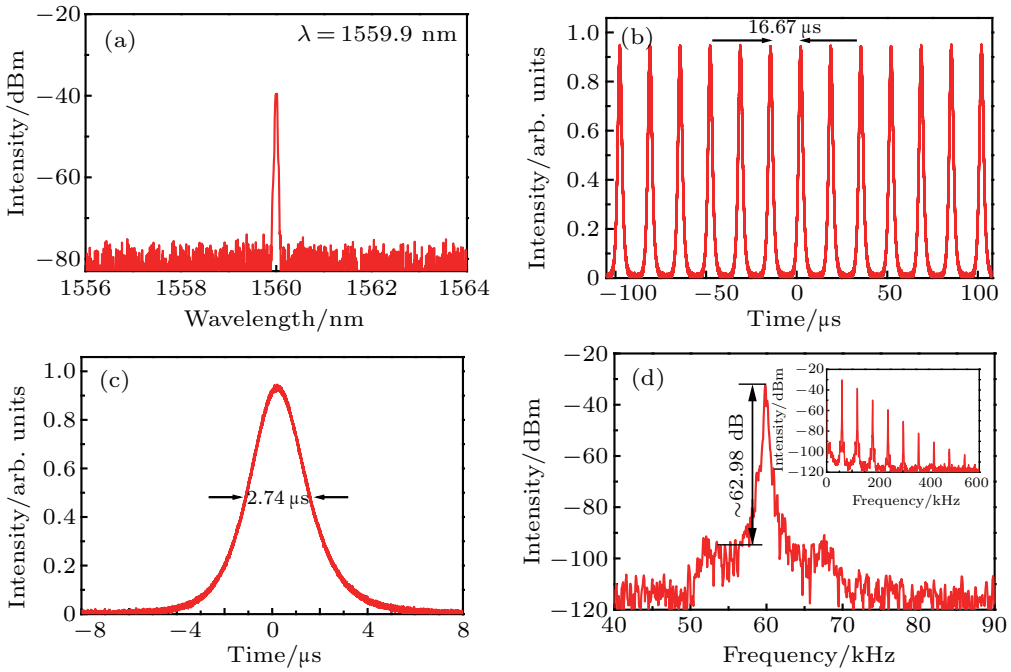


Fig. 7. The performance of the output pulse at a pump power of 100 mW. (a) Emission spectrum of single wavelength. (b) Pulse trains. (c) Single-pulse shape. (d) RF spectrum at $f = 60$ kHz; inset: RF spectrum over a large range of 600 kHz.

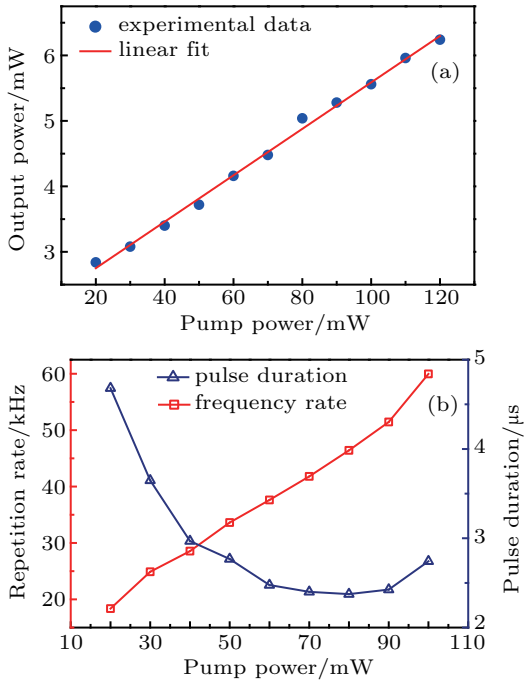


Fig. 8. The properties of the single wavelength pulse: (a) output power as a function of pump power; (b) pulse repetition rate and pulse duration as a function of pump power.

3.3. Dual-wavelength output

In the experiment, when we change the polarization state of the circulating by adjusting the PC, the pulse train can be observed in the oscilloscope with the dual-wavelength displayed on the OSA when the pump power increases to 5 mW. However, the pulse train is unstable because of the low pump power. To the best of our knowledge, the SA has a modulation depth. When the pump power is under 15 mW, the modulation is unstable and the pump power is too low to provide enough energy to generate a stable pulse train. As the pump power increases to 15 mW, stable passively Q-switched performance is achieved and the output power increases linearly as the pump power increases, which is illustrated in Fig. 10(a). Simultaneously, similar phenomenons have been described in the previous articles.[45,46] To gain a stable dual-wavelength, the pump power continues to increase. At a pump power of 15 mW, we obtain a stable dual-wavelength Q-switched laser. Figure 9(a) shows the dual-wavelength at the pump power of 35 mW, and the output pulse has two peak wavelengths 1559.7 nm and 1560.3 nm with the 3-dB bandwidth of 0.04 nm and 0.03 nm, respectively. As illustrated in Fig. 9(b), the interval of the pulse trains is 27.33 μs with the full width at half maximum (FWHM) of 5.66 μs (Fig. 9(c)). Figure 9(d) displays the RF spectrum which demonstrates the temporal stability of the passively Q-switched pulse with a signal-to-noise ratio of ∼ 58.72 dB.

Figure 10(a) illustrates the linear fit of the output power and pump power, and Fig. 10(b) displays the repetition rate, which increases from 19.21 kHz to 48.94 kHz as the pump power increases from 15 mW to 50 mW.

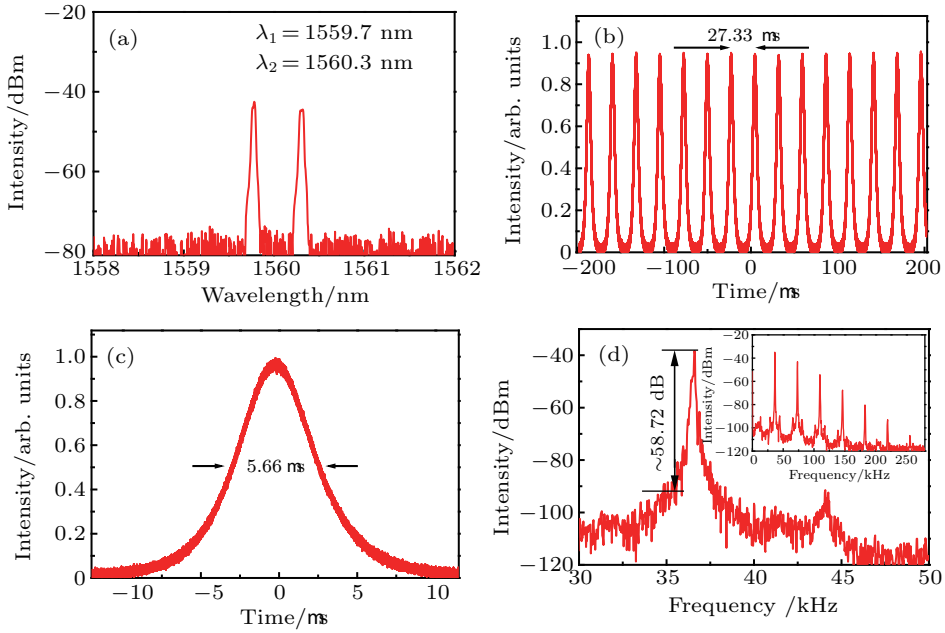


Fig. 9. The properties of pulse at the power pump of 35 mW. (a) Emission spectrum of dual-wavelength. (b) Pulse trains. (c) Single pulse shape. (d) RF spectrum of the dual-wavelength at $f = 36.6$ kHz; inset: RF spectrum over a large range of 280 kHz.

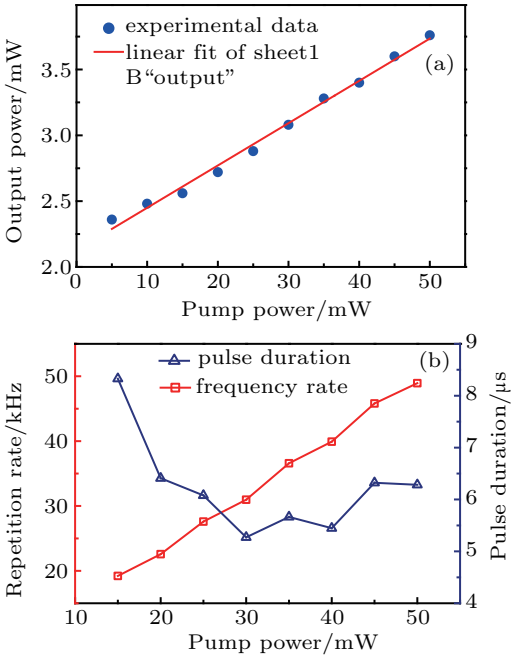


Fig. 10. The properties of the dual-wavelength pulse. (a) The output power as a function of pump power. (b) Pulse repetition rate and pulse duration as a function of pump power.

4. Conclusion and perspectives

In summary, the new 2D material $FePS_3$ has been successfully prepared and employed in a passively Q-switched erbium-doped fiber laser. By repeated experiments, we confirm that the single wavelength pulse signal can always be received when the pump power is in the range of 20 mW to 120 mW. Meanwhile, the dual-wavelength pulse has been achieved by adjusting the state of the PC. The $FePS_3$ film SA is sandwiched between two fiber ferrules to be used as a passively Q-switched device.

Under the condition of single wavelength pulse, the minimum pulse duration of Q-switched pulse is about 2.37 μs and the repetition rate can be varied from 18.36 kHz to 59.98 kHz, which changes completely as the pump power increases. When the pump power is 100 mW, the central wavelength is 1559.9 nm and the signal-to-radio of RF spectrum is measured to be 62.98 dB, which shows high stability of the passively Q-switched pulse. Under the condition of dual-wavelength pulse, the minimum pulse duration is about 5.27 μs with 8.33 μs as the maximum duration. For the repetition rate, it changes from 19.21 kHz to 48.94 kHz as the pump power increases. Moreover, one of the central wavelength is 1559.7 nm and another is 1560.3 nm with the pump power at 25 mW. At the same time, the signal-to-noise radio of RF spectrum is measured to be 58.72 dB. The experiment demonstrates that the new 2D material $FePS_3$ served as SA provides a valid method to realize passively Q-switched laser. The highlight is the achievement of a dual-wavelength pulse, which can be applied extensively in industrial processing and medical devices.

Acknowledgment

We off our thanks for the support provided by the Suzhou Institute of Nano-bionics, Nano-tech and Platform for Characterization & Test, Chinese Academy of Sciences (CAS).

References

[1] Fermann M E and Hartl I 2013 *Nat. Photon.* **7** 868
[2] Gillen R and Maultzsch J 2017 *IEEE J. Sel. Top. Quantum Electron.* **23** 1
[3] Yu S, Wu X, Wang Y, Guo X and Tong L 2017 *Adv. Mater.* **29** 1606128
[4] Zhang H, He J, Wang Z, Hou J, Zhang B, Zhao R, Han K, Yang K, Nie H and Sun X 2016 *Opt. Mater. Express* **6** 2328

[5] Mao D, Li M, Cui X, Zhang W, Lu H, Song K and Zhao J 2018 *Opt. Commun.* **406** 254
[6] Xie Y, Kong L, Qin Z, Xie G and Zhang J 2016 *Opt. Eng.* **55** 4
[7] Sotor J, Sobon G, Kowalczyk M, Macherzynski W, Paletko P and Abramski K M 2015 *Opt. Lett.* **40** 3885
[8] Wang F 2017 *Chin. Phys. B* **26** 034202
[9] Liu W J, Liu M L, Liu B, Quhe R G, Lei M, Fang S B, Teng H and Wei Z Y 2019 *Opt. Express* **27** 6689
[10] Liu W J, Liu M L, OuYang Y, Hou H R, Lei M and Wei Z Y 2018 *Nanotechnology* **29** 394002 6
[11] Shahzad F, Alhabeb M, Hatter C B, Anasori B, Man Hong S, Koo C M and Gogotsi Y 2016 *Science* **353** 1137
[12] Naguib M, Mochalin V N, Barsoum M W and Gogotsi Y 2014 *Adv. Mater.* **26** 992
[13] Wang C, Peng Q Q, Fan X W, Liang W Y, Zhang F, Liu J and Zhang H 2018 *Chin. Phys. B* **27** 094214
[14] Lee J and Lee J H 2018 *Chin. Phys. B* **27** 094219
[15] Tang Y, Wright L G, Charan K, Wang T, Xu C and Wise F W 2016 *Optica* **3** 948
[16] Wang Y, Xie G, Xu X, Di J, Qin Z, Suomalainen S, Guina M, Härkönen A, Agnesi A, Griebner U, Mateos X, Loiko P and Petrov V 2016 *Opt. Mater. Express* **6** 131
[17] Soref R 2015 *Nat. Photon.* **9** 358
[18] Rudy C W, Digonnet M J F and Byer R L 2014 *Opt. Fiber Technol.* **20** 642
[19] Geng J, Wang Q, Lee Y and Jiang S 2014 *IEEE J. Sel. Top. Quantum Electron.* **20** 150
[20] Bao Q L, Zhang H, Yang J X, Wang S, Tong D Y, Jose R, Ramakrishna S, Lim C T and Loh K P 2010 *Adv. Funct. Mater.* **20** 782
[21] Martinez A and Sun Z 2013 *Nat. Photon.* **7** 842
[22] Tuo M, Xu C, Mu H, Bao X, Wang Y, Xiao S, Ma W, Li L, Tang D, Zhang H, Premaratne M, Sun B, Cheng H M, Li S, Ren W and Bao Q 2018 *ACS Photon.* **5** 1808
[23] Kadir N A A, Ismail E I, Latiff A A, Ahmad H, Arof H and Harun S W 2017 *Chin. Phys. Lett.* **34** 014202
[24] Chen Y, Jiang G, Chen S, Guo Z, Yu X, Zhao C, Zhang H, Bao Q, Wen S, Tang D and Fan D 2015 *Opt. Express* **23** 12823
[25] Gao L, Xu J Y, Zhu Z Y, Hu C X, Zhang L, Wang Q and Zhang H L 2016 *Nanoscale* **8** 15132
[26] Ren Y, Qin Z, Xie G, Qiao Z, Ma J, Yuan P, Qian L, Wang S, Yu C and Hu L 2018 *Int. J. Opt.* **2018** 8060415 6
[27] Wang X T, Cui Y, Li T, Lei M, Li J B and Wei Z M 2019 *Adv. Opt. Mater.* **7** 1801274 17
[28] Luo Z C, Liu M, Luo A P and Xu W C 2018 *Chin. Phys. B* **27** 094215
[29] Zhu W, Gan W, Muhammad Z, Wang C, Wu C, Liu H, Liu D, Zhang K, He Q, Jiang H, Zheng X, Sun Z, Chen S and Song L 2018 *Chem. Commun.* **54** 4481
[30] Mayorga-Martinez C C, Sofer Z, Sedmidubsky D, Huber S, Eng A Y S and Pumera M 2017 *ACS Appl. Mater. Interfaces* **9** 12563
[31] Hu J, Zhang C, Meng X, Lin H, Hu C, Long X and Yang S 2017 *J. Mater. Chem. A* **5** 5995
[32] Du K Z, Wang X Z, Liu Y, Hu P, Utama M I B, Gan C K, Xiong Q and Kloc C 2016 *ACS Nano* **10** 1738
[33] Liu M, Tang R, Luo A P, Xu W C and Luo Z C 2018 *Photon. Res.* **6** C1
[34] Fuentealba P, Cortes C, Manzur J, Paredes-Garcia V, Venegas-Yazigi D, Silva I D A, de Santana R C, Magon C J and Spodine E 2017 *Dalton Trans.* **46** 14373
[35] Fuentealba P, Paredes-Garcia V, Venegas-Yazigi D, Silva I D A, Magon C J, de Santana R C, Audebr, N, Manzur J and Spodine E 2017 *RCS Adv.* **7** 33305
[36] Dangol R, Dai Z, Chaturvedi A, Zheng Y, Zhang Y, Khang Ngoc D, Li B, Zong Y and Yan Q 2018 *Nanoscale* **10** 4890
[37] Xiang H, Xu B, Xia Y, Yin J and Liu Z 2016 *Rsc Adv.* **6** 89901
[38] Danovich M, Aleiner I L, Drummond N D and Fal'ko V I 2017 *IEEE J. Sel. Top. Quantum Electron.* **23** 1
[39] Zhong L, Chen X and Qi J 2017 *Phys. Chem. Chem. Phys.* **19** 15388
[40] Pei Q, Wang X, Zou J and Mi W 2018 *J. Mater. Chem. C* **6** 8092
[41] Ahmad H, Ruslan N E, Ali Z A, Reduan S A, Lee C S J, Shaharuddin R A, Nayan N and Ismail M A 2016 *Opt. Commun.* **381** 85
[42] Hu Q, Li P, Zhang B, Liu B, Wang L and Chen X 2018 *Appl. Opt.* **57** 8242
[43] Long G, Zhang T, Cai X, Hu J, Cho C W, Xu S, Shen J, Wu Z, Han T, Lin J, Wang J, Cai Y, Lortz R, Mao Z and Wang N 2017 *ACS Nano* **11** 11330
[44] Wang X, Du K, Liu Y Y F, Hu P, Zhang J, Zhang Q, Owen M H S, Lu X, Gan C K, Sengupta P, Kloc C and Xiong Q 2016 *2D Mater.* **3** 031009
[45] Zhang H N and Liu J 2016 *Opt. Lett.* **41** 1150
[46] Su Y L, Huang X N, Hu H, Wen Y, Xie X P, Si J H, Wang Y S and Zhao W 2019 *Laser Phys.* **29** 065101 5